

Article

Quinoline-Malononitrile-Based Aggregation-Induced Emission Probe for Monoamine Oxidase Detection in Living Cells

Chuthamat Duangkamol^{1,2}, Sirilak Wangngae¹, Sirawit Wet-osot³ , Onnicha Khaikate¹, Kantapat Chansaenpak⁴, Rung-Yi Lai^{1,*}  and Anyanee Kamkaew^{1,*} 

¹ School of Chemistry, Institute of Science, Suranaree University of Technology, Nakhon Ratchasima 30000, Thailand

² Division of Basic and Medical Sciences, Faculty of Allied Health Sciences, Pathumthani University, Pathum Thani 12000, Thailand

³ Medical Life Science Institute, Department of Medical Sciences, Ministry of Public Health, Nonthaburi 11000, Thailand

⁴ National Nanotechnology Center, National Science and Technology Development Agency, Thailand Science Park, Pathum Thani 12120, Thailand

* Correspondence: ryilai@sut.ac.th (R.-Y.L.); anyanee@sut.ac.th (A.K.)

Abstract: A quinoline-malononitrile (QM)-based aggregation-induced emission probe was developed to detect MAOs in cells through an enzymatic reaction followed by β -elimination. After being incubated at 37 °C, QM-NH₂ responded to the MAO enzymes with great specificity and within just 5 min. This 5 min responsive mechanism was fast, with the limit of detection (LOD) at 5.49 and 4.76 $\mu\text{g mL}^{-1}$ for MAO-A and MAO-B, respectively. Moreover, QM-NH₂ displayed high enzyme specificity even in the presence of high concentrations of biological interferences, such as oxidizing and reducing agents, biothiols, amino acids, and glucose. Furthermore, QM-NH₂ demonstrated biocompatibility as the cells retained more than 70% viability when exposed to QM-NH₂ at concentrations of up to 20 μM . As a result, QM-NH₂ was used to detect MAO-A and MAO-B in SH-SY5Y and HepG2 cells, respectively. After 1h incubation with QM-NH₂, the cells exhibited enhanced fluorescence by about 20-fold. Moreover, the signal from cells was reduced when MAO inhibitors were applied prior to incubating with QM-NH₂. Therefore, our research recommends using a QM probe as a generic method for producing recognition moieties for fluorogenic enzyme probes.

Keywords: AIE; activity-based fluorescence probe; MAO; enzymatic detection; AIEgen



Citation: Duangkamol, C.; Wangngae, S.; Wet-osot, S.; Khaikate, O.; Chansaenpak, K.; Lai, R.-Y.; Kamkaew, A. Quinoline-Malononitrile-Based Aggregation-Induced Emission Probe for Monoamine Oxidase Detection in Living Cells. *Molecules* **2023**, *28*, 2655. <https://doi.org/10.3390/molecules28062655>

Academic Editors: Wenbo Wu, Zheng Zhao, Haoke Zhang, Fang Hu and Youhong Tang

Received: 8 February 2023

Revised: 7 March 2023

Accepted: 13 March 2023

Published: 15 March 2023



Copyright: © 2023 by the authors. Licensee MDPI, Basel, Switzerland. This article is an open access article distributed under the terms and conditions of the Creative Commons Attribution (CC BY) license (<https://creativecommons.org/licenses/by/4.0/>).

1. Introduction

Monoamine oxidases A and B (MAO-A and MAO-B) have attracted considerable interest from the pharmaceutical and biochemical communities since 50 years ago [1–4]. For instance, malonic acid's neurodegenerative toxicity and striatal damage can be considerably reduced by MAO inhibition, whereas MAO overexpression can lead to mitochondrial damage and an imbalance in oxidoreduction, which can result in neuronal death and brain damage [5]. MAOs are a flavoprotein that plays an important role in regulating tissue that catalyzes oxidation of monoamine to form the corresponding imine, followed by hydrolysis to an aldehyde [6]. There are specific inhibitors, clorgyline for MAO-A and pargyline for MAO-B [7]. MAO-A is a key target for being a primary cause of neuropsychiatric and depressive disorders, whereas MAO-B is strongly associated with a number of neurodegenerative diseases [8–11]. The specific detection of each MAO is thus critical for a better understanding of their functions in complex biosystems.

Quinoline-malononitrile (QM) was introduced to the original family as an aggregation-induced emission (AIE) building block, which is extremely helpful in understanding the molecular structure–property relationship [12]. Guo et al. developed an emitter named ED with an impressive alternative approach to modify the typical π -electron acceptor in

dicyanomethylene-4*H*-pyran chromophore (DCM) derivatives [13]. Many DCM derivatives have previously been reported due to their unique intramolecular charge transfer (ICT) and excellent opto-electronic properties. In general, the DCM chromophore has the typical Donor- π -Acceptor (D- π -A) property with a broad absorption band as a result of an ultra-fast ICT process [14]. However, due to the severe aggregation-caused quenching (ACQ) effect, conventional DCM derivatives can only be used as dopant emitters [15,16]. Strong face-to-face stacking with a typical ACQ effect occurs in the solid state as a result of the strong π - π interaction between the aromatic rings of DCM. On the other hand, the addition of an *N*-ethyl group to the acceptor of QM effectively suppresses the close stacking of molecules in its aggregate process [12]. Because of the aqueous physiological environment, water-soluble AIE systems are highly desirable for tracing important biological species.

Fluorescent materials are now crucial for biological investigation and clinical diagnosis since they offer dynamic and quantitative information about imaging biomolecules [17–19]. Because AIE materials exhibit turn-on fluorescence in aggregation while dim in solution [20], the fascinating AIE phenomenon in particular offers prospective advantages, especially in biosensing applications [21–24]. Due to its great sensitivity, the use of AIE fluorescent probes in conjunction with confocal imaging techniques is increasingly becoming more and more common for monitoring MAOs in living biosystems [25–27]. The existing fluorescence probes are made to detect either MAO-A [25–27] or MAO-B [28,29] with AIE properties. For example, the methyl substituent on tetraphenylethylene (TPE) derivatives (*trans*-TPEM), among the six produced probes, exhibits a notable increase in fluorescence when MAOs are added with selectivity toward MAO-A [30]. In a different work, TPE was synthesized with an extended conjugation to thiophene to create TPE-TPys, which had a perfect D- π -A structure and a high level of positive charges [31]. These compounds demonstrated outstanding MAO-A specificity, high-efficiency photosensitivity, and mitochondrial targeting. To the best of our knowledge, none of the QM-based MAO fluorescent turn-on probes are AIE-active probes [4,30]. As a result, it would be interesting to investigate the AIE probe's ability to detect MAOs through the reaction-based sensing scheme (Figure 1B).

In this study, we developed an AIE probe based on the QM building block, **QM-NH₂**, which has reduced fluorescence and may be used to detect MAOs in cells since it has a responsive moiety consisting of propylamine. When the probe binds to MAOs after oxidation and hydrolysis, it undergoes β -elimination, releasing **QM-OH**, an AIE agent that activates the fluorescence signal. Our probe provided a fast response to MAO activity, within 5 min, in both solution and living cells. It was also available for real-time and in situ imaging with good photostability, high resolution, and long-term tracking capabilities. We believe that our **QM-NH₂** overcomes the inherent shortcomings of ACQ fluorophores and offers better properties than the conventional AIEgens, even though the majority of available AIE probes always emphasize the improper aggregation in both the aqueous system and lipophilic organelle before binding to the specific receptor.

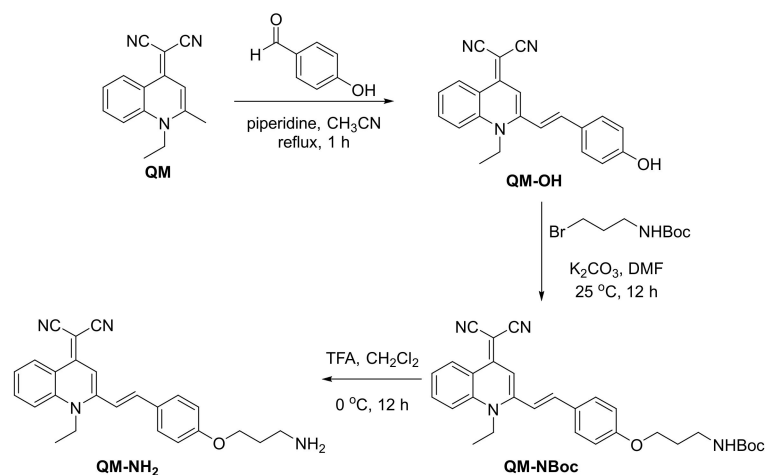
2. Results and Discussions

2.1. Synthesis

The synthetic steps of an enzyme-activatable AIE-active probe (**QM-NH₂**) based on AIEgen **QM-OH** with a *para*-phenolic group protected by propylamine, an MAO-triggered unit, are described in Figure 1A. Starting with an AIE building block, quinoline-malononitrile (**QM**), a signal reporter, was prepared from *N*-methylated 2-methylquinoline and propane dinitrile [31]. Then, **QM** was condensed with the 4-hydroxybenzaldehyde in the presence of piperidine under the reflux condition to obtain the AIEgen **QM-OH** [32] in a moderate yield, 57%. After that, **QM-OH** was directly conjugated with the *t*-Boc-protected primary bromopropylamine to produce the compound **QM-NBoc** in 68% yield. Finally, the deprotection of **QM-NBoc** with trifluoroacetic acid at low temperature produced the amino-ended **QM-NH₂** at 56% yield as an orange solid. Detailed synthetic procedure (Scheme S1) and characterization (¹H-NMR, ¹³C-NMR, and HRMS) are depicted in the Supplementary Materials.

The general concept of fluorescence enzyme assays is that compounds are not fluorescence substrates until they are acted on by their enzymes of interest. The amount of light produced by the reaction of **QM-NH₂** with the liberated substrate, most commonly **QM-OH**, can then be linked to the activity of the enzyme of interest. Because MAO oxidizes primary, secondary, and tertiary acyclic amines to produce iminium intermediates, which are hydrolyzed to the corresponding aldehydes (Figure 1B), we reasoned that such iminium and/or aldehyde derivatives could aid in the liberation of **QM-OH** via a β -elimination process.

(A) Synthesis of a probe for MAOs detection



(B) Proposed reaction mechanism

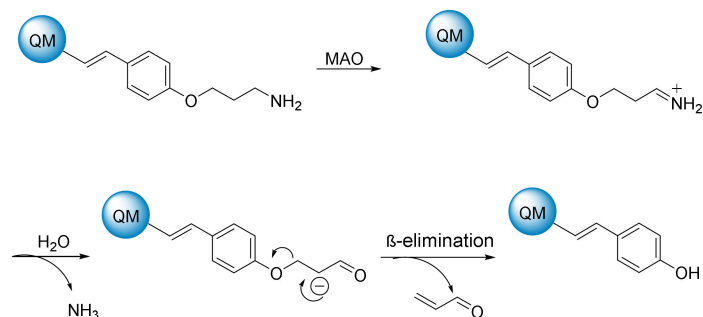


Figure 1. (A) Synthetic scheme of **QM-NH₂**. (B) Proposed reaction mechanism of **QM-OH** generation from **QM-NH₂**. MAOs oxidize the amine of **QM-NH₂** to form the imine followed by hydrolysis to generate the aldehyde. Finally, the aldehyde undergoes β -elimination to generate **QM-OH**.

2.2. Photophysical Properties

QM-NH₂ and **QM-OH** (the proposed product after the MAO enzymatic reaction) were tested for their photophysical properties. Every compound has an absorbance in HEPES buffer (pH 7.4) that ranges from 300–550 nm with two peaks at 370 and 450 nm, which is characteristic of **QM** (Figure 2A). Compared to **QM-NH₂**, **QM-OH** has a substantially greater emission (8-fold higher) in HEPES buffer, as shown by the emission spectrum, peaking at 559 nm (Figure 2B) with a large Stokes shift of 114 nm. Fluorescence quantum yields for **QM-NH₂** and **QM-OH** in the buffer are calculated as 0.003 and 0.025, respectively, confirming high fluorescent emissions for **QM-OH**. Then, the aggregation-induced emission (AIE) property of **QM-OH** was investigated in tetrahydrofuran (THF)–water mixtures with different water fractions (f_w). As shown in Figure 2C, the emission intensity changes of **QM-OH** were negligible as f_w was increased from 0% to 80%. When the f_w reached 90%, the fluorescence intensity increased sharply by about 360-fold from pure THF,

indicating the strong AIE property of **QM-OH** in the medium with high water contents. On the other hand, the **QM-NH₂** probe exhibited non-emissive reactions in all water fractions as demonstrated in Figure 2D. These results suggest that **QM-NH₂** could potentially detect MAO through the fluorescence enhancement phenomenon in the aggregated form.

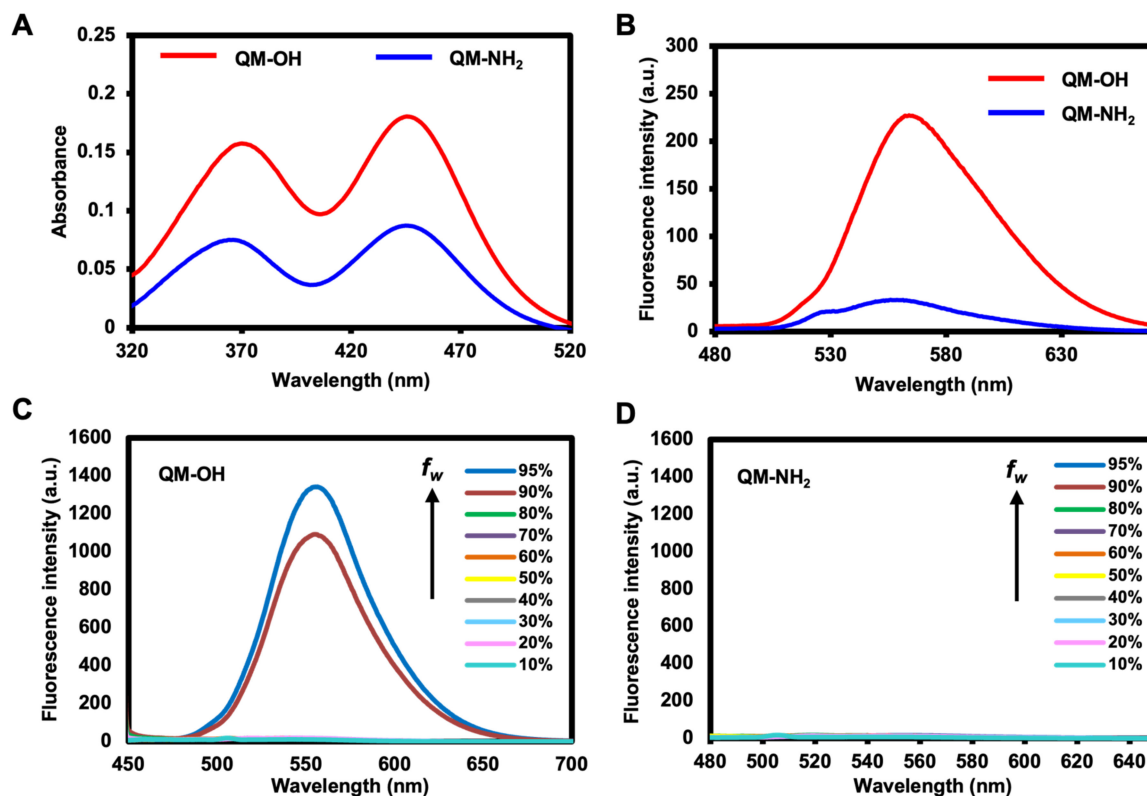


Figure 2. (A) Absorption spectra of **QM-NH₂** and **QM-OH** in HEPES buffer. (B) Emission spectra (excited $\lambda = 445$ nm) of **QM-NH₂** and **QM-OH** in HEPES buffer. Aggregation-induced emission property of (C) **QM-OH** and (D) **QM-NH₂** investigated in tetrahydrofuran (THF)–water mixtures with different water fractions (f_w) in which THF is a good solvent and water is a poor solvent.

2.2.1. Fluorescence Responses of **QM-NH₂** to MAOs

The response of **QM-NH₂** for MAO-A and MAO-B was then investigated. The enzymatic reactions were performed in 100 mM HEPES buffer (pH 7.4) at 37 °C for 5 min. Figure 3A showed the fluorescent spectroscopic properties of **QM-NH₂** and its response to MAOs. Four different scenarios were tested under the physiological condition: (i) **QM-OH** alone, (ii) **QM-OH** in the presence of MAO-A or MAO-B, (iii) **QM-NH₂** in the presence of MAO-A or MAO-B, and (iv) **QM-NH₂** alone. Probe **QM-NH₂** (condition iv) exhibited almost no emission in the HEPES buffer, but when it reacted with MAOs (condition iii), a strong emission enhancement at 559 nm was observed. The emission spectra of **QM-NH₂** in the presence of MAOs are similar to those of **QM-OH** in the presence of MAOs, implying that **QM-OH** is the product of the reactions. Furthermore, the responses of **QM-NH₂** to MAOs are dose-dependent as the fluorescence increments were directly proportional to the enzyme concentrations (Figure 3B,C). The linear relationships between the fluorescent signals and the enzyme concentrations were observed at the 0–20 $\mu\text{g}/\text{mL}$ range of MAO-A and MAO-B (Figure 3D,E). The detection limits of **QM-NH₂** were calculated as 5.49 and 4.76 $\mu\text{g}/\text{mL}$ for MAO-A and MAO-B, respectively.

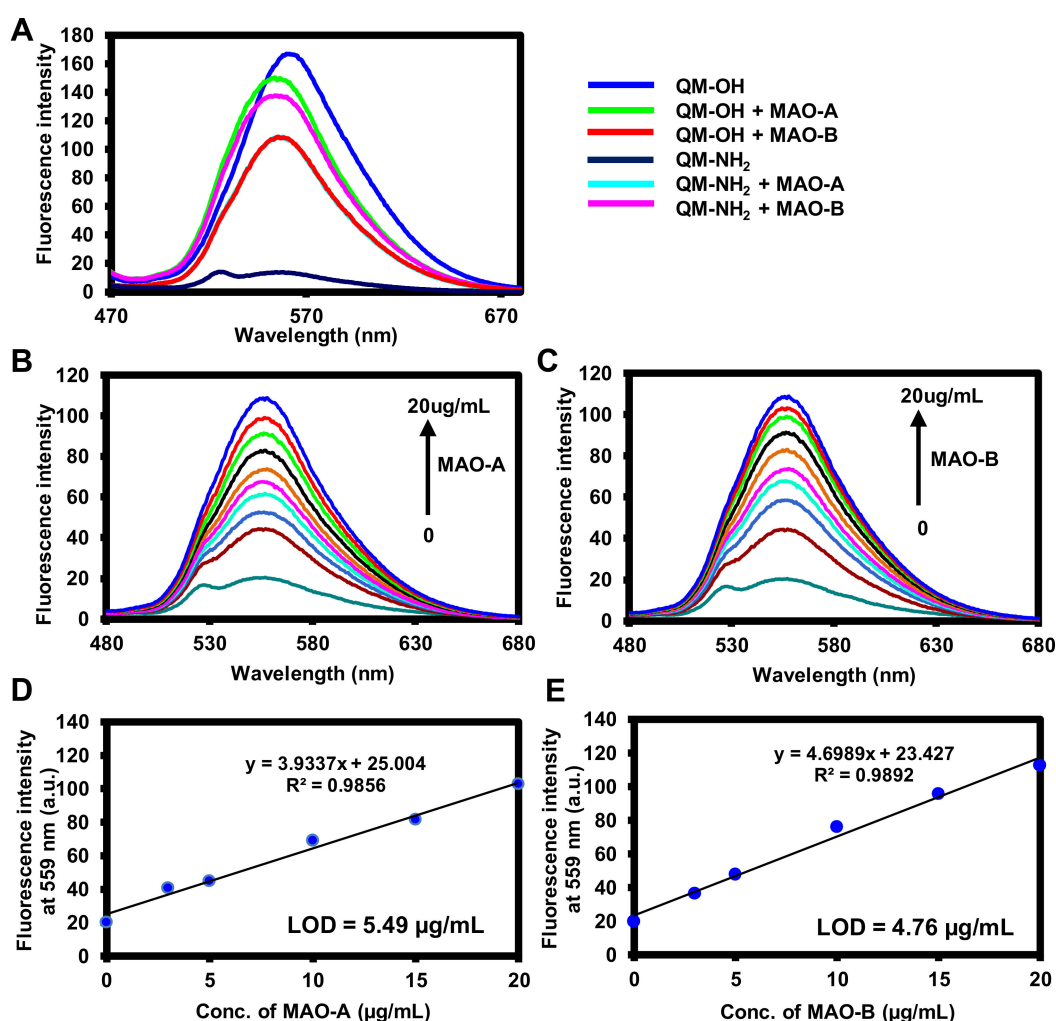


Figure 3. (A) Fluorescence spectra of 10 µM QM-NH₂ (navy blue line) and QM-NH₂ after reaction with 20 µg/mL of MAO-A (cyan line) and MAO-B (red line). The synthesized QM-OH (10 µM, blue line) and its reaction with 20 µg/mL of MAO-A (green line) and MAO-B (pink line) were tested as the controls. Fluorescence responses of QM-NH₂ reacted with (B) MAO-A and (C) MAO-B at concentrations ranging from 0–20 µg/mL. The data were recorded in the enzymatic assay buffer (100 mM HEPES, pH = 7.4 with 5% glycerol and 1% DMSO) at 37 °C after 5 min incubation. Linear fluorescence intensity responses of QM-NH₂ reacting with various concentrations of (D) MAO-A and (E) MAO-B.

2.2.2. HPLC Analysis of the Enzymatic Reaction

To identify the product of QM-NH₂ after MAO-catalyzed reaction, the reaction mixtures of MAO-A and MAO-B were subjected to HPLC analysis as shown in Figure 4. The chromatograms of QM-NH₂ and QM-OH are displayed in Figure 4A,B, while the ones for the MAO-A- and MAO-B-catalyzed reactions in the existence of QM-NH₂ are demonstrated in Figure 4C,D, respectively. The presence of the peak at 4.89 min retention time suggested the formation of QM-OH after the enzymatic reactions. To further confirm the peak identity, the standard of QM-OH was spiked into each reaction mixture to show the comigration as manifested in Figure 4E,F. Furthermore, the eluent of each peak was collected for mass spectrometric analysis to confirm its identity. According to HPLC and mass spectrometric analyses, it was proven that the enzymes (MAO-A and MAO-B) oxidized QM-NH₂, followed by hydrolysis and β-elimination to generate QM-OH.

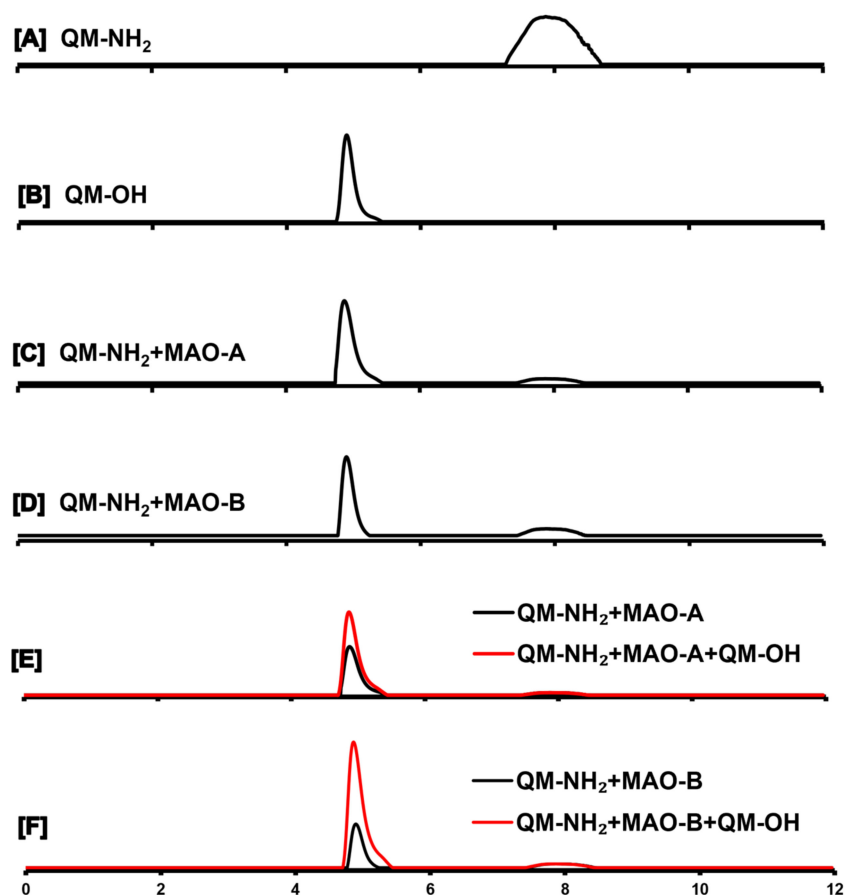


Figure 4. HPLC chromatograms of different reaction systems: (A) 100 μM **QM-NH₂**; (B) 100 μM **QM-OH**; (C) the reaction of 100 μM **QM-NH₂** treated with 20 $\mu\text{g/mL}$ MAO-A for 5 min; (D) the reaction of 100 μM **QM-NH₂** treated with 20 $\mu\text{g/mL}$ MAO-B for 5 min; (E) comigration of **QM-NH₂** + MAO-A reaction with **QM-OH** spiking; and (F) comigration of **QM-NH₂** + MAO-B reaction with **QM-OH** spiking. Detection: UV-vis (400 nm) detector. Flow rate: 0.7 mL/min. Temperature: 25 $^{\circ}\text{C}$. Injection volume: 40 μL . Mobile phase (isocratic elution): MeOH/water = 70/30 (*v/v*) for 12 min.

2.2.3. Selectivity of **QM-NH₂** toward MAOs

To investigate the selectivity of **QM-NH₂**, the probe was incubated with cations, anions, urea, amino acids, or glutathione to observe if the fluorescence turned on or not. As expected, the fluorescence intensities at 559 nm produced by MAO-A and MAO-B are significantly higher than that produced by other analytes, as shown in Figure 5. Furthermore, when **QM-NH₂** was exposed to MAOs at high concentrations of oxidizable interferences, such as amino acids (alanine and cysteine) and glucose, the fluorescence intensity did not change significantly (Figure S1). According to these findings, the probe **QM-NH₂** has a high selectivity for MAOs.

Following that, we investigated the effects of temperature factors on fluorescence intensity at 559 nm. As seen in Figure S2, the fluorescence changes upon the addition of enzymes increased along with the enhancement of reaction temperatures from 25 to 37 $^{\circ}\text{C}$ as the enzyme activity increased. However, at 45 $^{\circ}\text{C}$, the fluorescence change dropped, which could be the result of enzyme denaturation at high temperatures. Therefore, the optimum temperature for these enzymatic reactions is 37 $^{\circ}\text{C}$, which is a physiological condition. Next, we tested the stability of probes **QM-NH₂** and **QM-OH** by incubating the probes in HEPES buffer, pH = 7.4. According to Figure S3, the probes **QM-NH₂** and **QM-OH** in HEPES buffer only showed a slight change in fluorescence signal, indicating that probe **QM-NH₂** and **QM-OH** were stable in the solution for at least 48 h. These results

demonstrated that determining MAOs using the probe **QM-NH₂** was suitable for biological applications advantageous in physiological conditions.

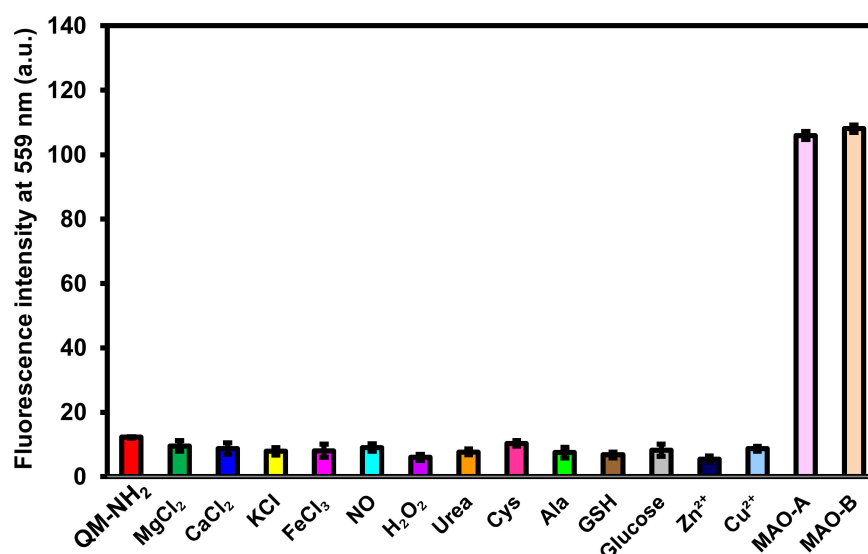


Figure 5. Fluorescence response of **QM-NH₂** (10 μ M) after 5 min of incubation at 37 $^{\circ}$ C with various analytes: MgCl₂ (2.5 mM), CaCl₂ (2.5 mM), KCl (150 mM), FeCl₃ (100 μ M), NO (100 μ M), H₂O₂ (100 μ M), urea (20 mM), cysteine (1 mM), alanine (1 mM), reducing glutathione (GSH, 1 mM), glucose (10 mM), Zn²⁺ (1 mM), Cu²⁺ (1 mM), MAO-A (20 μ g/mL), and MAO-B (20 μ g/mL). The results are expressed as the mean SD (n = 3). $\lambda_{ex/em}$ = 455/559 nm.

2.2.4. Interactions of **QM-NH₂** and MAOs Visualized by Molecular Docking

Molecular docking is a powerful tool for describing the interactions between a compound and a protein receptor. In silico docking of **QM-NH₂** with MAO-A and MAO-B was used to estimate the preferred orientation of the compound inside the active site using AutoDock 4.2. The computational results showed that **QM-NH₂** fits both MAO-A and MAO-B in their active site regions (MAO-A: Tyr69, Ala111, Ile207, Phe208, Val210, Gln215, Cys323, Ile335, Phe352, Tyr444) (Figure 6A) and (MAO-B: Tyr60, Pro102, Phe103, Leu167, Leu171, Ile198, Gly205, Gln206, Ile316, Tyr326, Leu328, Tyr435) (Figure 6C). The distances of the carbon adjacent to the terminal amine and the N5 atom of FAD are 6.3 \AA in MAO-A and 5.5 \AA in MAO-B, respectively, suggesting that **QM-NH₂** was oriented in the direction of FAD in close proximity [33]. Additionally, to verify the used docking method, the docking comparative experiments were performed using tyramine, a non-specific inhibitor of both MAO isozymes (Figure 6B,D). The results showed that **QM-NH₂** could bind to both MAO-A and MAO-B in a similar orientation to tyramine. The binding free energy calculations and residue contacts are summarized in Table S1.

2.3. Cellular Assays

Next, the biocompatibility of **QM-NH₂** was tested in two cancer cell lines, human neuroblastoma (SH-SY5Y) and human liver (HepG2) cells. The cells were treated with various concentrations of **QM-NH₂** (0, 2.5, 5, 10, 20, 30, and 50 μ M) for 24 h. The comparative cell viability was determined by the standard MTT assay [34]. According to Figure 7A, when SH-SY5Y cells, which overexpress MAO-A [35], and HepG2 cells, which overexpress MAO-B [36], were exposed to **QM-NH₂**, the cell viability was still greater than 70%. Higher concentrations, i.e., 30–50 μ M, however, caused the cell viability to start declining quickly. This might be because of the aggregation at high concentrations. As a result, it is safe to apply doses in the 1 to 10 μ M range in cellular tests.

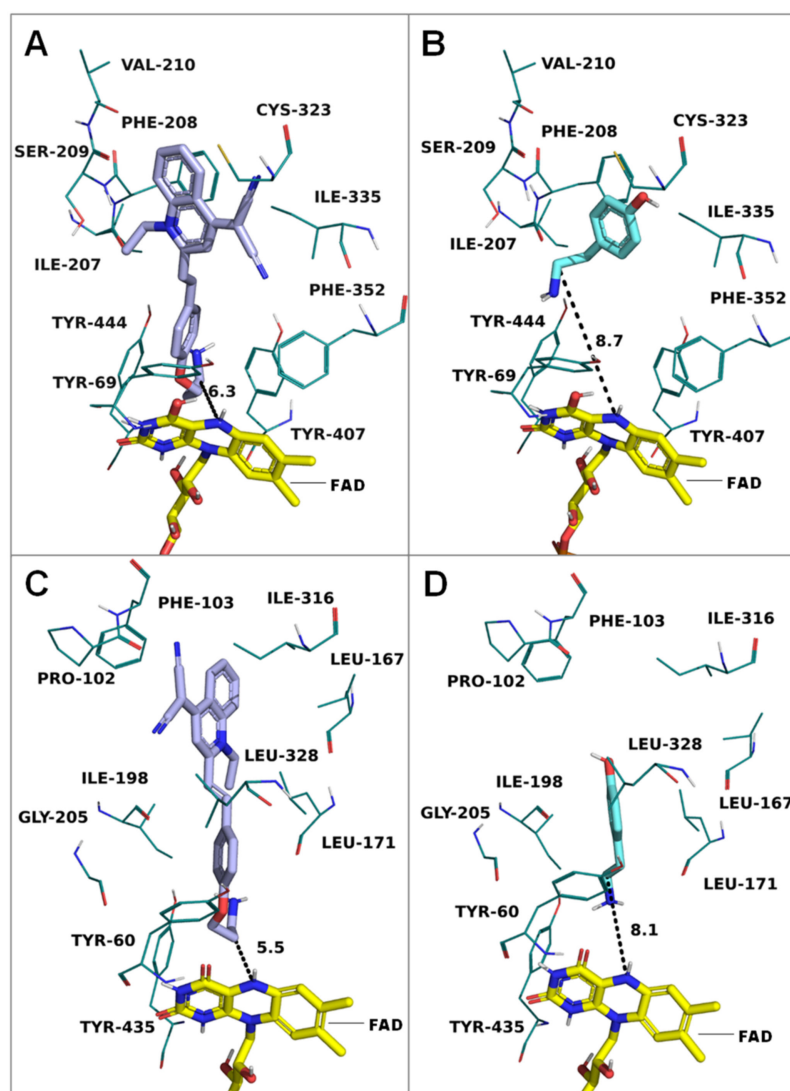


Figure 6. Calculated docking poses of **QM-NH₂** and tyramine in the active site of MAO-A (PDB: 2BXR) and MAO-B (PDB: 2V5Z) crystal structures: (A,B) docking poses of **QM-NH₂** and tyramine with MAO-A, respectively; (C,D) docking poses of **QM-NH₂** and tyramine with MAO-B, respectively. FAD is shown in yellow sticks; important residues of MAO are depicted as deep cyan lines, and distance measurements are shown in dashed lines.

Subsequently, the capability of **QM-NH₂** for fluorescence imaging of endogenous MAO-A and MAO-B activity in SH-SY5Y and HepG2 cells was investigated. Time-dependent intracellular enzyme activity was performed to track the fluorescence signal of **QM-OH** generated from the MAOs-catalyzed reaction. Within a few minutes, the signal was visible from the cells, and as time increased, the fluorescence enhanced (Video in Data Availability Statement). For live cell imaging, we captured the green fluorescence observed from both cell types and the signals grew stronger over time (Figure 7B and Figure S4). Furthermore, the cancer cells fluoresced brighter in the first hour compared to the healthy cell, human foreskin fibroblasts (HFF) (Figure S5), which corresponds to the higher MAO levels expressed in cancer cells compared to normal cells [37]. As the reaction time was extended, it appeared that both malignancy and normal cells glowed brightly (Figure S5), suggesting that the ideal detection time is within the first hour.

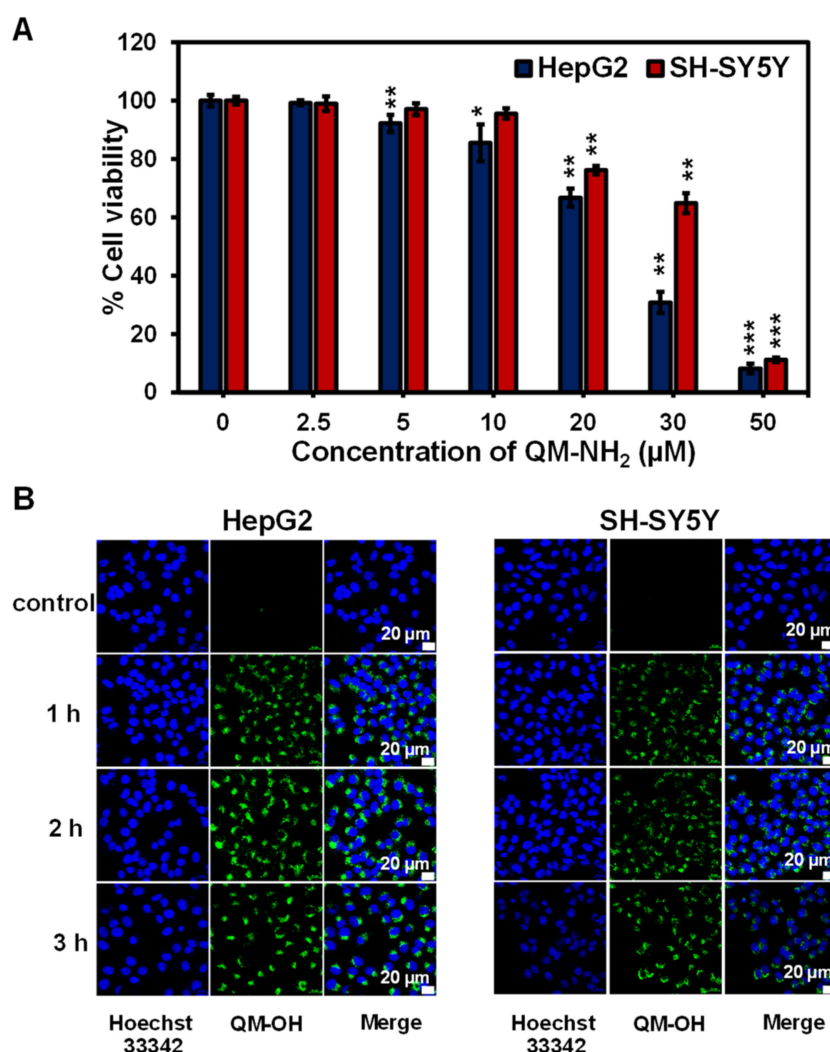


Figure 7. (A) Relative cell viability of SH-SY5Y and HepG2 cells treated with QM-NH₂ at different concentrations for 24 h. Statistical analysis is based on T-test (* $p < 0.05$, ** $p < 0.01$, *** $p < 0.001$). (B) Confocal images of time-dependent enzymatic reactions for the detection of QM-OH in SH-SY5Y and HepG2 cells were obtained using a laser scanning confocal microscope (Nikon A1Rsi, 63× oil immersed optics). The cells were incubated with 10 μM of QM-NH₂ for 1–3 h, nucleus is shown in blue as Hoechst 33342 signal (excitation laser = 405 nm, emission band 450/25 nm); QM-OH can be detected as green fluorescence (excitation laser = 488 nm, emission band 515/30 nm).

To broaden the application of QM-NH₂ in the detection of MAOs in various cancer cell types, including cervical (HeLa), lung (A549), and breast (MCF-7) cells, the cells were exposed to the probe for 3 h before being fixed and imaged. Bright green fluorescence was observed from all the cells, implying that QM-NH₂ is compatible with all cancer types. In addition, it is intriguing that the light is still discernible after cell fixation, suggesting the potential application in immunostaining (Figure S6).

Next, to confirm the selectivity toward MAO, the cells were pretreated with MAO inhibitors, clorgyline, and pargyline, before incubating with QM-NH₂. As shown in Figure 8, clorgyline suppressed endogenous MAO-A activity in SH-SY5Y cells and reduced fluorescence signals by 52%. In contrast, pargyline suppressed MAO-B activity in HepG2 cells, resulting in a 10% drop in fluorescence when compared to cells not treated with the inhibitor. This suggested that QM-NH₂ could be selective to MAO in living cells.

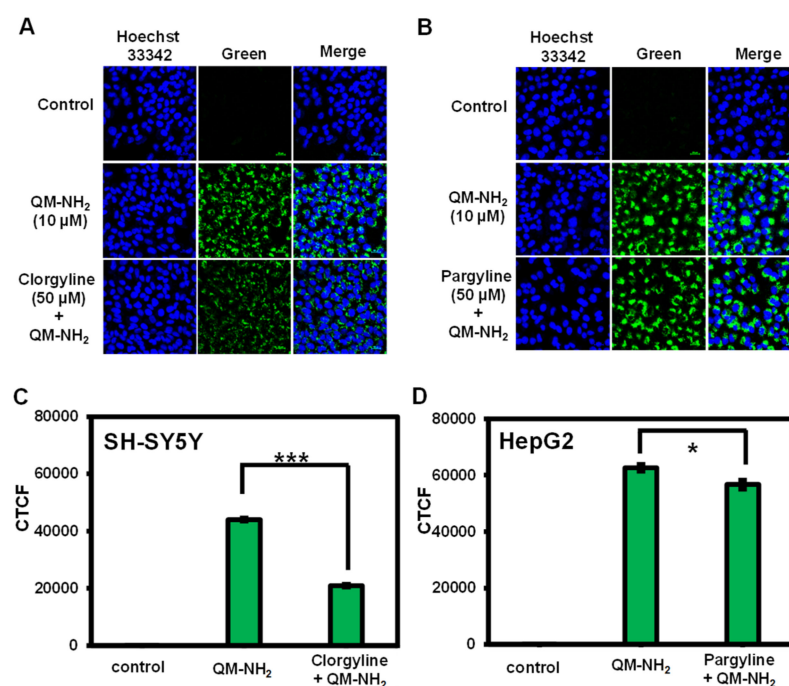


Figure 8. Confocal images of (A) SH-SY5Y and (B) HepG2 cells treated with QM-NH₂ in the absence and presence of potent MAO inhibitors (MAO-A: clorgyline and MAO-B: pargyline). (C,D) Quantitative fluorescent intensity of images in (A,B), respectively, represented as corrected total cell fluorescence (CTCF), which were quantified using ImageJ and represent the mean ± SD (from three independent experiments, 30 cells/set, respectively). Scale bar = 20 μm. Statistical analysis is based on T-test (* $p < 0.05$, *** $p < 0.001$).

3. Materials and Instruments

The absorption and fluorescence spectra were collected using a UV–vis spectrophotometer (Agilent Technologies Cary 300, Santa Clara, CA, USA) and a fluorescence spectrophotometer (PerkinElmer LS55, Liantrisant, UK). Nuclear magnetic resonance (NMR) spectroscopy (¹H and ¹³C NMR) was performed at room temperature on a Bruker instrument (500 MHz) spectrometer (Rheinstetten, Germany) with TMS as an internal reference. Under the ESI condition, high-resolution mass spectrometry (HRMS) spectra were recorded on a mass spectrometer. Prior to use, all glassware was oven dried. All reagents and solvents were purchased commercially (Sigma Aldrich, TCI (Tokyo, Japan), Carlo Erba (Emmendingen, Germany), Acros (Geel, Belgium), Merck (Rahway, NJ, USA)) and used without further purification. Purifications by column chromatography were carried out using silica gel for chromatography (Carlo Erba) as a stationary phase. Analytical thin layer chromatography (TLC) was performed on TLC Silica gel 60 F254 (Merck) and visualized under a UV cabinet. Human monoamine oxidase A and monoamine oxidase B were purchased from Sigma Aldrich.

3.1. UV–vis and Fluorescence Spectroscopic Methods

In all experiments, the stock solutions (10 mM) of QM-OH and QM-NH₂ were prepared in DMSO. The fluorescence spectra of QM-NH₂ (10 μM) with MAOs in 100 mM HEPES buffer (pH 7.4) were measured after 5 min incubation at 37 °C. For AIE property investigation, QM-OH and QM-NH₂ were dissolved in tetrahydrofuran (THF)–water mixtures with different water fractions (*fw*) from 0% to 95%. UV–vis absorption and fluorescence spectra were performed in a quartz cell with a 1 cm path length and recorded on a UV–vis spectrophotometer (T80+ UV–vis spectrometer, PG Instruments Ltd., Lutterworth, UK) and a spectrofluorometer (JASCO FP-8300, Japan, Tsukuba), respectively. The fluorescence spectra were recorded at $\lambda_{\text{ex}} = 445 \text{ nm}$.

3.2. MAO Assays

Generally, in an assay volume of 50 μL , 0–20 μg of protein from microsomes containing MAO-A or MAO-B (Sigma-Aldrich, Taufkirchen, Germany) were incubated with 10 μM of the probe **QM-NH₂** in the buffer (100 mM HEPES containing 5% glycerol and 1% DMSO, pH 7.4) at 37 °C for 5 min. The reaction mixtures were analyzed by the fluorescence spectroscopic method or high-performance liquid chromatography (HPLC). The HPLC instrument is Agilent 1100 (Waldbronn, Germany). The column is ZORBAX Eclipse XDB-C18 (4.6 mm \times 150 mm, 5 μm ID).

3.3. Cell Culture

Human lines, neuroblastoma (SH-SY5Y), hepatocellular carcinoma (HepG2), cervical adenocarcinoma (HeLa), lung adenocarcinoma (A549), breast cancer (MCF-7), and foreskin fibroblasts (HFF) were cultured on 75 cm³ culture flasks in complete media according to the ATCC (American Type Culture Collection) protocols. All cells were cultured in a humidified incubator at 37 °C under 5% CO₂.

3.4. Cell Viability Assay

The cells were seeded into 96-well cell culture plates at 2×10^4 cells/well and incubated for 24 h for cell viability testing. Following that, cell culture media were replaced with media containing various concentrations of **QM-NH₂** (0, 2.5, 5, 10, 20, 30, and 50 μM). Cell viability was determined using the standard MTT protocol after 24 h of incubation. In brief, the cells were washed three times with PBS before being treated for 2 h with methylthiazolyldiphenyl-tetrazolium bromide (20 μL , 0.5 mg/mL, Sigma-Aldrich). The culture media was then replaced with DMSO, and cell viability was determined using a microplate reader (BMG Labtech/SPECTROstar Nano, Offenburg, Germany) to detect the absorption of the resulting formazan at 560 nm.

3.5. Time-Dependent Internalization

Cells were seeded at a density of 7×10^3 cells per well in an 8-well chambered coverglass with non-removable wells (Nunc Lab-Tek II Chamber Slide) and incubated for 24 h. After that, cell culture media were removed and the cells were pre-treated with 10 μM of **QM-NH₂** solution in DMEM with 5% FBS for 1, 2, 3, 6, and 24 h. After incubation, the cells were washed three times with 0.01 M PBS and stained with 0.5 mg/mL of Hoechst 33342 containing media. The cells were then imaged under a laser scanning confocal microscope (LSCM, Nikon A1Rsi). The resulting **QM-OH** was visualized using a 488 nm laser excitation and emission filter of 515/30 nm. Hoechst 33342 was detected using an excitation laser = 405 nm and emission filter of 450/25 nm. A 60 \times oil immersion objective lens was used.

3.6. Time Course Live Cell Imaging

Approximately 1×10^4 cells of HepG2 were seeded on a cell dish for 24 h. Then, 10 μM of **QM-NH₂** solution in DMEM with 5% FBS was added to the cell dish, followed by a prompt VDO recording for 30 min by 60 \times oil immersion objective lens of laser scanning confocal microscope (Nikon A1Rsi) with 405 nm and 488 nm lasers.

3.7. Cell Fixation Assay

Approximately 1×10^4 cells were seeded on an 8-well chambered coverglass for 24 h. Then, the cells were incubated with 10 μM of **QM-NH₂** for 3 h. After incubation, the cells were washed three times with 0.01 M PBS, followed by the addition of 4% paraformaldehyde (PFA) and incubation for 20 min at room temperature. The cells were fixed on the coverslip containing DAPI mounting media. Then, the cells were visualized under 60 \times oil immersion objective lens by laser scanning confocal microscope (Nikon A1Rsi) with 405 nm and 488 nm lasers.

3.8. Inhibition Assay

At approximately 1×10^4 cells/well, cells were seeded on an 8-well chambered coverglass (LabTek, Nunc) and incubated in completed media for 24 h. After that, SH-SY5Y and HepG2 cells were treated with clorgyline and pargyline (50 μ M), respectively, for 1 h prior to incubation with QM-NH₂ (10 μ M) for another 3 h. After incubation, the cells were washed three times with PBS and treated with 0.5 mg/mL of Hoechst 33342 containing media before being imaged by LCSM.

For the corrected total cell fluorescence (CTCF), an outline was drawn around each cell using ImageJ, and the circularity, area, and mean fluorescence were assessed, as well as numerous surrounding background readings. CTCF was calculated as follows:

CTCF = integrated density - (area of selected cell \times mean fluorescence of background readings).

This CTCF was then compared to the mean CTCF of nearby interphase cells in the same field of view, with the findings shown as a fold increase above interphase values. Three background regions were chosen for each image to correct against autofluorescence.

3.9. Statistical Analysis

Data are expressed as the mean of at least four individual observations with the standard deviation (mean \pm SD) from three independent experiments ($n = 3$). Paired Student's *t*-test analysis was used for the statistical analysis. *p*-values < 0.05 were considered to indicate significance (* $p < 0.05$, ** $p < 0.01$, *** $p < 0.001$).

3.10. Molecular Docking

A docking study was performed by Autodock 4.2 [38] to discover the binding mode of the protein and ligands. The X-ray crystal structures of the human monoamine oxidase A in complex with clorgyline (PDB: 2BXR) and human monoamine oxidase B in complex with safinamide (PDB: 2V5Z) were retrieved from the Protein Data Bank database and submitted to prepare the receptor wizard. The protein receptor was prepared by the deletion of water molecules and addition of polar hydrogens. The FAD coenzyme was not removed during the docking process. Docking parameter files (gpf and dpf) were generated using the AutoDock tools (ADT) software as setting grid box size of 70/70/70 around center 21.417/2.033/5.763 for MAO-A and 53.317/154.718/26.810 for MAO-B. Docking was performed with 100 runs and a maximum of 2,500,000 evaluations and standard parameters. The protein–ligand complexes and distance measurement (between N5 of FAD and the carbon adjacent to the amine group) were displayed by PyMol [39] to identify the potency of recognition.

4. Conclusions

In summary, we developed an AIE fluorogenic probe that undergoes the enzymatic reaction to detect MAO-A and MAO-B inside living cells in a timely manner (within 5 min). The QM-based AIE probe, QM-NH₂, was created by combining the substituted phenol with propylamine as a recognition moiety for MAOs. The spectrophotometric analysis revealed that the enzymatic reaction product, QM-OH, had an 8-fold fluorescence enhancement. The HPLC analysis confirmed that QM-OH is the final product after the enzymatic reaction. A series of intracellular imaging experiments of MAOs in cancer cells overexpressing MAO-A (SH-SY5Y) and MAO-B (HepG2) confirms QM-NH₂'s ability to detect MAOs in complex biological systems. As QM-NH₂ is the first QM-based AIE probe to detect MAOs, we believe that our strategy could pave the way for the development of AIE probes for other enzyme activities.

Supplementary Materials: The following supporting information can be downloaded at: <https://www.mdpi.com/article/10.3390/molecules28062655/s1>. General procedure for the synthesis of QM-OH and QM-NH₂ and compound characterizations; Figure S1: Fluorescence response of QM-NH₂ to MAOs in the presence of interferences; Figure S2: Effects of temperature on the fluorescence intensity of QM-NH₂ and QM-OH, Figure S3: Stability of QM-NH₂ and QM-OH in HEPES

buffer; Figure S4: Confocal images of time-dependent enzymatic reaction detection of **QM-NH₂** in SH-SY5Y and HepG2 cells; Figure S5: Confocal images of SH-SY5Y, HepG2, and HFF cells treated with **QM-NH₂** for 1–2 h; Figure S6: Confocal images of various cancer cells treated with **QM-NH₂** for 3 h.; Table S1: Docking results.

Author Contributions: Conceptualization: A.K. and R.-Y.L.; Data curation: C.D., S.W., S.W.-o., O.K., K.C., A.K. and R.-Y.L.; Funding acquisition: A.K. and R.-Y.L.; Investigation: C.D., S.W., S.W.-o. and O.K.; Methodology: A.K., R.-Y.L., C.D., S.W. and S.W.-o.; Project administration: A.K.; Resources: K.C. and R.-Y.L.; Supervision: A.K., R.-Y.L. and K.C.; Validation: R.-Y.L. and A.K.; Visualization: C.D., S.W., S.W.-o., O.K., R.-Y.L. and A.K.; Writing—original draft: C.D., S.W., S.W.-o., R.-Y.L. and A.K.; Writing—review and editing: all authors. All authors have read and agreed to the published version of the manuscript.

Funding: A. Kamkaew received funding from Suranaree University of Technology (SUT), Thailand Science Research and Innovation (TSRI) and National Science, Research and Innovation Fund (NSRF) (NRIIS number 4325918). A. Kamkaew and R.-Y. Lai received funding from SUT, TSRI, and the National Research Council of Thailand (N41A640150 and N42A650326).

Institutional Review Board Statement: Not applicable.

Informed Consent Statement: Not applicable.

Data Availability Statement: Data are contained within the article or Supplementary Materials. Video is available at: <https://youtu.be/4eDFGoZFYvU> (accessed on 12 March 2023).

Conflicts of Interest: The authors declare no conflict of interest.

Sample Availability: Samples of **QM-OH** and **QM-NH₂** are available from the authors.

References

1. Shih, J.C.; Chen, K.; Ridd, M.J. Role of MAO A and B in neurotransmitter metabolism and behavior. *Pol. J. Pharmacol.* **1999**, *51*, 25–29. [[PubMed](#)]
2. Shih, J.C.; Chen, K.; Ridd, M.J. Monoamine oxidase: From genes to behavior. *Annu. Rev. Neurosci.* **1999**, *22*, 197–217. [[CrossRef](#)] [[PubMed](#)]
3. Edmondson, D.E.; Mattevi, A.; Binda, C.; Li, M.; Hubalek, F. Structure and mechanism of monoamine oxidase. *Curr. Med. Chem.* **2004**, *11*, 1983–1993. [[CrossRef](#)] [[PubMed](#)]
4. Yang, Z.; Li, W.; Chen, H.; Mo, Q.; Li, J.; Zhao, S.; Hou, C.; Qin, J.; Su, G. Inhibitor structure-guided design and synthesis of near-infrared fluorescent probes for monoamine oxidase A (MAO-A) and its application in living cells and in vivo. *Chem. Commun.* **2019**, *55*, 2477–2480. [[CrossRef](#)] [[PubMed](#)]
5. Mattson, M.P. Apoptosis in neurodegenerative disorders. *Nat. Rev. Mol. Cell Biol.* **2000**, *1*, 120–129. [[CrossRef](#)]
6. Maragos, W.F.; Young, K.L.; Altman, C.S.; Pocernich, C.B.; Drake, J.; Butterfield, D.A.; Seif, I.; Holschneider, D.P.; Chen, K.; Shih, J.C. Striatal damage and oxidative stress induced by the mitochondrial toxin malonate are reduced in clorgyline-treated rats and MAO-A deficient mice. *Neurochem. Res.* **2004**, *29*, 741–746. [[CrossRef](#)]
7. Geha, R.M.; Rebrin, I.; Chen, K.; Shih, J.C. Substrate and inhibitor specificities for human monoamine oxidase A and B are influenced by a single amino acid. *J. Biol. Chem.* **2001**, *276*, 9877–9882. [[CrossRef](#)]
8. Youdim, M.B.; Buccafusco, J.J. CNS Targets for multi-functional drugs in the treatment of Alzheimer's and Parkinson's diseases. *J. Neural. Transm.* **2005**, *112*, 519–537. [[CrossRef](#)]
9. Wang, C.C.; Billett, E.; Borchert, A.; Kuhn, H.; Ufer, C. Monoamine oxidases in development. *Cell. Mol. Life Sci.* **2013**, *70*, 599–630. [[CrossRef](#)]
10. Murphy, D.L.; Lipper, S.; Slater, S.; Shiling, D. Selectivity of clorgyline and pargyline as inhibitors of monoamine oxidases A and B in vivo in man. *Psychopharmacology* **1979**, *62*, 129–132. [[CrossRef](#)]
11. McDermott, R.; Tingley, D.; Cowden, J.; Frazzetto, G.; Johnson, D.D. Monoamine oxidase A gene (MAOA) predicts behavioral aggression following provocation. *Proc. Natl. Acad. Sci. USA* **2009**, *106*, 2118–2123. [[CrossRef](#)]
12. Guo, Z.; Yan, C.; Zhu, W.H. High-Performance Quinoline-Malononitrile Core as a Building Block for the Diversity-Oriented Synthesis of AIEgens. *Angew. Chem. Int. Ed.* **2020**, *59*, 9812–9825. [[CrossRef](#)]
13. Shi, C.; Guo, Z.; Yan, Y.; Zhu, S.; Xie, Y.; Zhao, Y.S.; Zhu, W.; Tian, H. Self-assembly solid-state enhanced red emission of quinolinemalononitrile: Optical waveguides and stimuli response. *ACS Appl. Mater. Interfaces* **2013**, *5*, 192–198. [[CrossRef](#)]
14. Guo, Z.; Zhu, W.; Tian, H. Dicyanomethylene-4H-pyran chromophores for OLED emitters, logic gates and optical chemosensors. *Chem. Commun.* **2012**, *48*, 6073–6084. [[CrossRef](#)]
15. Díaz, I.; Kokkoli, E.; Terasaki, O.; Tsapatsis, M. Surface structure of zeolite (MFI) crystals. *Chem. Mater.* **2004**, *16*, 5226–5232. [[CrossRef](#)]
16. Chen, C.-T. Evolution of red organic light-emitting diodes: Materials and devices. *Chem. Mater.* **2004**, *16*, 4389–4400. [[CrossRef](#)]

17. Wu, X.; Li, Z.; Chen, X.-X.; Fossey, J.S.; James, T.D.; Jiang, Y.-B. Selective sensing of saccharides using simple boronic acids and their aggregates. *Chem. Soc. Rev.* **2013**, *42*, 8032–8048. [[CrossRef](#)]
18. Chan, J.; Dodani, S.C.; Chang, C.J. Reaction-based small-molecule fluorescent probes for chemoselective bioimaging. *Nat. Chem.* **2012**, *4*, 973–984. [[CrossRef](#)]
19. Myochin, T.; Hanaoka, K.; Komatsu, T.; Terai, T.; Nagano, T. Design strategy for a near-infrared fluorescence probe for matrix metalloproteinase utilizing highly cell permeable boron dipyrromethene. *J. Am. Chem. Soc.* **2012**, *134*, 13730–13737. [[CrossRef](#)]
20. Guo, Z.; Shao, A.; Zhu, W.-H. Long wavelength AIEgen of quinoline-malononitrile. *J. Mater. Chem. C* **2016**, *4*, 2640–2646. [[CrossRef](#)]
21. Luo, J.; Xie, Z.; Lam, J.W.; Cheng, L.; Chen, H.; Qiu, C.; Kwok, H.S.; Zhan, X.; Liu, Y.; Zhu, D.; et al. Aggregation-induced emission of 1-methyl-1,2,3,4,5-pentaphenylsilole. *Chem. Commun.* **2001**, *18*, 1740–1741. [[CrossRef](#)] [[PubMed](#)]
22. Pramanik, S.; Bhalla, V.; Kumar, M. Hexaphenylbenzene-based fluorescent aggregates for ratiometric detection of cyanide ions at nanomolar level: Set-reset memorized sequential logic device. *ACS Appl. Mater. Interfaces* **2014**, *6*, 5930–5939. [[CrossRef](#)]
23. An, B.K.; Kwon, S.K.; Jung, S.D.; Park, S.Y. Enhanced emission and its switching in fluorescent organic nanoparticles. *J. Am. Chem. Soc.* **2002**, *124*, 14410–14415. [[CrossRef](#)] [[PubMed](#)]
24. Gao, F.; Liu, G.; Qiao, M.; Li, Y.; Yi, X. Biosensors for the Detection of Enzymes Based on Aggregation-Induced Emission. *Biosensors* **2022**, *12*, 953. [[CrossRef](#)] [[PubMed](#)]
25. Chen, G.; Yee, D.J.; Gubernator, N.G.; Sames, D. Design of optical switches as metabolic indicators: New fluorogenic probes for monoamine oxidases (MAO A and B). *J. Am. Chem. Soc.* **2005**, *127*, 4544–4545. [[CrossRef](#)]
26. Zhou, W.; Valley, M.P.; Shultz, J.; Hawkins, E.M.; Bernad, L.; Good, T.; Good, D.; Riss, T.L.; Klaubert, D.H.; Wood, K.V. New bioluminogenic substrates for monoamine oxidase assays. *J. Am. Chem. Soc.* **2006**, *128*, 3122–3123. [[CrossRef](#)]
27. Kim, D.; Sambasivan, S.; Nam, H.; Kim, K.H.; Kim, J.Y.; Joo, T.; Lee, K.H.; Kim, K.T.; Ahn, K.H. Reaction-based two-photon probes for in vitro analysis and cellular imaging of monoamine oxidase activity. *Chem. Commun.* **2012**, *48*, 6833–6835. [[CrossRef](#)]
28. Loo, L.S.; Tang, N.; Al-Haddawi, M.; Dawe, G.S.; Hong, W. A role for sorting nexin 27 in AMPA receptor trafficking. *Nat. Commun.* **2014**, *5*, 3176. [[CrossRef](#)]
29. Li, L.; Zhang, C.W.; Ge, J.; Qian, L.; Chai, B.H.; Zhu, Q.; Lee, J.S.; Lim, K.L.; Yao, S.Q. A Small-Molecule Probe for Selective Profiling and Imaging of Monoamine Oxidase B Activities in Models of Parkinson’s Disease. *Angew. Chem. Int. Ed.* **2015**, *54*, 10821–10825. [[CrossRef](#)]
30. Li, L.L.; Li, K.; Liu, Y.H.; Xu, H.R.; Yu, X.Q. Red emission fluorescent probes for visualization of monoamine oxidase in living cells. *Sci. Rep.* **2016**, *6*, 31217. [[CrossRef](#)]
31. Han, X.; Yang, X.; Zhang, Y.; Li, Z.; Cao, W.; Zhang, D.; Ye, Y. A novel activatable AIEgen fluorescent probe for peroxynitrite detection and its application in EC1 cells. *Sens. Actuators B Chem.* **2020**, *321*, 128510. [[CrossRef](#)]
32. Wang, M.; Yang, N.; Guo, Z.; Gu, K.; Shao, A.; Zhu, W.; Xu, Y.; Wang, J.; Prud’homme, R.K.; Guo, X. Facile Preparation of AIE-Active Fluorescent Nanoparticles through Flash Nanoprecipitation. *Ind. Eng. Chem. Res.* **2015**, *54*, 4683–4688. [[CrossRef](#)]
33. Li, L.; Zhang, C.W.; Chen, G.Y.; Zhu, B.; Chai, C.; Xu, Q.H.; Tan, E.K.; Zhu, Q.; Lim, K.L.; Yao, S.Q. A sensitive two-photon probe to selectively detect monoamine oxidase B activity in Parkinson’s disease models. *Nat. Commun.* **2014**, *5*, 3276. [[CrossRef](#)]
34. Van Meerloo, J.; Kaspers, G.J.; Cloos, J. Cell sensitivity assays: The MTT assay. *Methods Mol. Biol.* **2011**, *731*, 237–245.
35. Naoi, M.; Maruyama, W.; Akao, Y.; Yi, H.; Yamaoka, Y. Involvement of type A monoamine oxidase in neurodegeneration: Regulation of mitochondrial signaling leading to cell death or neuroprotection. In *Oxidative Stress and Neuroprotection*; Springer: Berlin, Germany, 2006; pp. 67–77.
36. Shih, J.C.; Chen, K. Regulation of MAO-A and MAO-B gene expression. *Curr. Med. Chem.* **2004**, *11*, 1995–2005. [[CrossRef](#)]
37. Aljanabi, R.; Alsous, L.; Sabbah, D.A.; Gul, H.I.; Gul, M.; Bardaweel, S.K. Monoamine Oxidase (MAO) as a Potential Target for Anticancer Drug Design and Development. *Molecules* **2021**, *26*, 6019. [[CrossRef](#)]
38. Morris, G.M.; Huey, R.; Lindstrom, W.; Sanner, M.F.; Belew, R.K.; Goodsell, D.S.; Olson, A.J. AutoDock4 and AutoDockTools4: Automated docking with selective receptor flexibility. *J. Comput. Chem.* **2009**, *30*, 2785–2791. [[CrossRef](#)]
39. Giacovazzo, C.; Capitelli, F.; Cuocci, C.; Ianigro, M. Direct methods and applications to electron crystallography. In *Microscopy, Spectroscopy, Holography and Crystallography with Electrons*; Hawkes, P.W., Merli, P.G., Calestani, G., Vittori-Antisari, M., Eds.; Elsevier: Amsterdam, The Netherlands, 2002; Volume 123, pp. 291–310.

Disclaimer/Publisher’s Note: The statements, opinions and data contained in all publications are solely those of the individual author(s) and contributor(s) and not of MDPI and/or the editor(s). MDPI and/or the editor(s) disclaim responsibility for any injury to people or property resulting from any ideas, methods, instructions or products referred to in the content.